Transient Temperature Probe Measurements

in a Mach 4 Nitrogen Jet

D R BUTTSWORTH

Faculty of Engineering and Surveying

University of Southern Queensland

Toowoomba, Qld, 4350

Australia

Email: buttswod@usq.edu.au

Fax: 61 7 4631 2526

T V JONES

Department of Engineering Science

University of Oxford

Oxford, OX1 3PJ

UK

Abstract

Stagnation temperature measurements have been obtained in a Mach 4 free jet of nitrogen using a technique based on transient thin film heat flux probe measurements. The uncertainty in the stagnation temperature measurements depends on the probe location within the jet but is typically around ±5K at the centre of the jet. The thin film heat flux probe technique also provides a measurement of the heat transfer coefficient of the thin film probes with an uncertainty of around ±4% at the centre of the jet. Pitot pressure measurements were also obtained within the jet. Analysis of the heat transfer coefficient results yields the Mach number and velocity profiles which are compared with results from the pitot probe measurements. Jet velocities identified using the thin film probe and the pitot probe techniques produce results with uncertainties of less than ±2% at the centre of the jet. Measurements of RMS stagnation temperature fluctuations indicate values of around 3K at the centre of the jet to more than 10K in the shear layer.

List of Symbols

c_p specific heat (assumed constant)

C Chapman-Rubesin parameter, Eq. (7)

D probe diameter

h convective heat transfer coefficient

k conductivity

K stagnation point velocity gradient, Eq. (6)

M Mach number

n exponent in power law viscosity and conductivity expressions

Nu Nusselt number, Eq. (3)

p pressure

Pr Prandtl number, Eq. (4)

q heat flux

R specific gas constant

Re probe Reynolds number, Eq. (5)

T temperature

u velocity

x distance from jet exit, or distance along probe surface from stagnation

y distance from jet centreline

γ ratio of specific heats

μ viscosity

ρ density

subscripts

e probe boundary layer edge

pit pitot

ref reference value in power law viscosity and conductivity expressions

w probe surface value

0 stagnation

∞ free stream, undisturbed by probe

1 Introduction

Stagnation temperature measurements are important in many experiments involving compressible flows. If stagnation temperature measurements at frequencies less than about 1kHz are required, then vented thermocouple probes or possibly exposed thermocouple probes (Vas 1972) may produce adequate results. However, for stagnation temperature measurements at frequencies higher than 1kHz, aspirating probes with imbedded hot wire devices (Ng and Epstein 1983) are often used. For aspirating probes of a practical size, the upper bandwidth for stagnation temperature measurements appears to be around 20kHz because of the need to establish a quasi-steady flow within the probe (VanZante et al. 1994).

For applications requiring stagnation temperature measurements at frequencies in excess of 20kHz, it may be possible to utilize the transient thin film heat flux probe approach that was introduced by Buttsworth and Jones (1998a). With this technique, transient thin film gauges can be operated at different surface temperatures in order to identify the stagnation temperature in a manner that is independent of the convective heat transfer coefficient of the probes. Previous applications of the transient thin film technique (Buttsworth and Jones 1998a,b; Buttsworth et al. 1998) have demonstrated its capacity for stagnation temperature measurements at bandwidths approaching 100kHz.

3

Although the probe discussed by Buttsworth and Jones (1998a) primarily measures the flow stagnation temperature, the technique can also yield convective heat transfer coefficient measurements. While the measurement of heat transfer coefficient has been alluded to and demonstrated in previous publications, the identification of probe-independent flow parameters from the heat transfer coefficient measurements has not been attempted in the previous work.

In the current article, the transient thin film heat flux gauge technique is applied to a Mach 4 free jet of nitrogen. Time-averaged flow stagnation temperature and probe convective heat transfer coefficient distributions are obtained at 4 locations downstream of a Mach 4 injector nozzle. Flow parameters such as the Mach number and velocity distributions are then identified from the probe convective heat transfer coefficient measurements and comparisons are made with results derived from pitot probe measurements. Stagnation temperature fluctuation measurements are also presented at the 4 locations downstream of the Mach 4 injector nozzle.

2 Temperature Probe

2.1 Thin Film Gauges

Transient thin film gauges have been used for many years in a variety of applications (Schultz and Jones 1973). Recent developments have extended the frequency response of thin film gauges down to dc without substantially compromising the simplicity of the transient thin technique (Piccini et al. 2000).

However, in the current application, platinum films were hand-painted onto the rounded end of fused quartz rods with a diameter of around 3mm, as illustrated in Fig. 1. Low resistance gold leads were also painted onto the quartz and the active film length was less than 1mm in each case. The films were operated in a constant current mode so that the voltage drop across each film indicated the film resistance and thus its temperature. The present technique requires heat flux measurements at different probe surface temperatures and these different temperatures were obtained using the heating unit shown in Fig. 1. Each film was calibrated over its full range of operating

temperatures and a quadratic temperature-resistance relationship was established for each film.

2.2 Basis of Measurement Technique

For moderate flow stagnation temperatures, it is reasonable to express the stagnation point heat flux as,

$$q = h(T_0 - T_w),\qquad(1)$$

where q is the heat flux, h is the heat transfer coefficient, T_0 is the flow stagnation temperature, and T_w is the temperature at the probe surface. It is appropriate that the stagnation temperature, rather than the recovery temperature, appears in Eq. (1) because the flow velocity in the vicinity of the stagnation point is very low (Buttsworth and Jones 1998b).

Provided h is independent of T_w, Eq. (1) indicates that it is possible to experimentally identify both the flow stagnation temperature and the convective heat transfer coefficient of the probes if the transient heat flux q is measured at two different probe temperatures T_w. However, three thin film probes were adopted in this work, as illustrated in Fig. 1, because the RMS analysis indicated that the equation governing the heat transfer fluctuations is a quadratic in T_0-T_w (see section 5.1).

2.3 Heat Transfer Coefficient Correlation

2.3.1 Correlation using Pitot Pressure

The thin film probe heat transfer coefficient measurements can be used to provide information on additional flow parameters provided a suitable correlation for h exists. Theoretical results (e.g., White 1991) suggest that the stagnation point heat transfer coefficient for a sphere at any Mach number can be correlated using,

$$Nu = 0.763 Pr^{0.4} Re^{0.5} C^{0.1} \left(\frac{KD}{u_\infty} \right)^{0.5}\qquad(2)$$

where,

5

$$Nu = \frac{hD}{k_e} \qquad (3)$$

$$Pr = \frac{c_p \mu_e}{k_e} \qquad (4)$$

$$Re = \frac{\rho_e u_\infty D}{\mu_e} \qquad (5)$$

$$K = \frac{du_e}{dx} \qquad (6)$$

$$C = \frac{\rho_w \mu_w}{\rho_e \mu_e}. \qquad (7)$$

A key parameter that is often measured in typical experiments is the pitot pressure, so it is convenient to rearrange the heat transfer coefficient in terms of the pitot pressure. Assuming a perfect gas, p_{pit} enters Eq. (2) through the Reynolds number (Eq. 5) using,

$$\rho_e = \frac{p_e}{RT_e} = \frac{p_{pit}}{RT_0}. \qquad (8)$$

The undisturbed free stream Mach number is,

$$M_\infty = \frac{u_\infty}{(\gamma R T_\infty)^{0.5}} \qquad (9)$$

and,

$$R = \frac{\gamma - 1}{\gamma} c_p. \qquad (10)$$

Hence, it is possible to rearrange the heat transfer coefficient in Eq. (2) with the aid of Eq. (8) to Eq. (10) as,

$$h = 0.763 D^{-0.5} f(M_\infty, \gamma) f(\text{thermophysical properties}) p_{pit}^{0.5} \qquad (11)$$

where

$$f(M_\infty, \gamma) = \gamma^{0.5} (\gamma - 1)^{-0.25} (M_\infty)^{0.5} \left(\frac{T_\infty}{T_0}\right)^{0.25} \left(\frac{KD}{u_\infty}\right)^{0.5} \qquad (12)$$

and

$$f(\text{thermophysical properties}) = c_p^{0.15} k_e^{0.6} \mu_e^{-0.1} C^{0.1} T_0^{-0.25} \qquad (13)$$

Although Eq. (2) is an elegant expression of the (nondimensional) stagnation point heat transfer coefficient, Eq. (11) relates the heat transfer coefficient to flow parameters that can be measured far more directly.

2.3.2 Temperature Sensitivity

To investigate the extent to which h is independent of T_w and T_0, the perfect gas relation is again adopted and for simplicity we approximate the viscosity and conductivity using a single power law exponent. Equation (13) then becomes

$$f(\text{thermophysical properties}) \approx c_p^{0.15} \frac{k_{ref}^{0.6}}{\mu_{ref}^{0.1}} T_{ref}^{-0.5n} T_w^{-0.1(1-n)} T_0^{0.4n-0.15}. \qquad (14)$$

White (1991) gives power law exponents of $n=0.67$ for the viscosity of nitrogen, and $n=0.74$ for the conductivity of nitrogen. Hence, the simplicity afforded by a single power law exponent is justified because these values differ from the mean value ($n=0.705$) by less than 5% which is comparable to the inherent accuracy of the power law approximations (White 1991).

For a given stagnation temperature, and taking $n=0.71$, Eq. (14) indicates that the heat transfer coefficient varies with the probe surface temperature according to $T_w^{-0.029}$. For the present experiments, where the probe temperatures varied between about 300K and 600K, the expected variation in convective heat transfer coefficient is around 2%. (The uncertainty in the actual value of the power law exponent does not affect this conclusion.) Thus the approach described in Section 2.2, which requires a constant value of heat transfer coefficient, is not severely compromised by the variation of h with T_w as the experimental uncertainties involved in the identification of h are larger than 2% (see Section 4.2).

For a given probe temperature, and again taking $n=0.71$, Eq. (14) indicates that the heat transfer coefficient varies with stagnation temperature according to $T_0^{0.13}$. Thus,

when estimating the heat transfer coefficient for a given range of flow conditions, variations in T_0 will have some effect. However, in the current application where the stagnation temperature across the jet varies by less than 5%, the heat transfer coefficient varies by less than 1% in response to these changes in stagnation temperature.

2.3.3 Mach Number Sensitivity

The sensitivity of the heat transfer coefficient to the flow Mach number is illustrated in Fig. 2 which was generated using Eq. (12) with $\gamma=1.4$. To obtain the result presented in Fig. 2, the temperature ratio T_∞/T_0 in Eq. (12) was evaluated using the normal isentropic expression, and the velocity gradient term was determined using expressions given by White (1991),

$$\frac{KD}{u_\infty} \approx 3(1-0.252M_\infty^2 - 0.0175M_\infty^4) \ \text{ for } M_\infty < 0.8 \qquad (15)$$

and

$$\frac{KD}{u_\infty} \approx \left(\frac{8\rho_\infty}{\rho_e}\right)^{0.5} \ \text{ for } M_\infty > 1.2 \qquad (16)$$

with an interpolation between Eq. (15) and Eq. (16) for $0.8 < M_\infty < 1.2$.

Experimental data indicates stagnation point velocity gradients consistently lower than predicted using Eq. (15) and (16) by about 10% for Mach numbers ranging from 0 to 5 (White 1991). This would lead an error in convective heat transfer coefficient of around 5% over the full range of Mach numbers considered in this work. However, the approach adopted in the present work was to adjust the effective probe diameter used in Eq. (11) according to the heat transfer coefficient measured in the jet core flow at $x=1$mm (see Section 4.3). This small correction eliminates the contribution of the apparent systematic errors in the velocity gradient correlations discussed above.

For subsonic flows, the heat transfer coefficient is a strong function of the Mach number but it is virtually independent of the Mach number for supersonic flows as

illustrated in Fig. 2. Thus, Eq. (12) indicates that it is not particularly critical to have a precise measurement of the flow Mach number in order to identify the convective heat transfer coefficient provided the flow is supersonic.

3 Free Jet and Probe Arrangement

Experiments were performed using the free jet arrangement illustrated in Fig. 3. The contoured Mach 4 injection nozzle had a throat diameter of 9.42mm and was designed using the method of characteristics. The nozzle exit diameter was 29.5mm and the lip thickness was 0.5mm. The injection nozzle was located in the test section of the Oxford University Gun Tunnel. Nitrogen was supplied to the Mach 4 nozzle from an unheated Ludwieg tube. Prior to a run, the test section was evacuated to approximately 1.2kPa, and the slug of nitrogen in the Ludwieg tube was isolated from the low pressure test section by a fast-acting valve.

A short time after opening the fast-acting valve, a pressure rise was indicated by the injection pressure transducer and the injection static pressure measured about 3mm upstream of the nozzle lip decreased during flow establishment and then increased back up to the steady injection value – see Fig. 4a. The Ludwieg tube filling pressure was chosen so that the steady injection static pressure was approximately the same as the initial test section pressure. The matching of injection static pressure and test section pressure remains somewhat uncertain because during the probe traverse of the jet, the test section pressure transducer registered about 1.05kPa – lower than the initial test section pressure prior to flow establishment, Fig. 4a.

The thin film and pitot pressure probes were initially located above the centreline of the free jet and were driven across the jet at around 70ms after the fast-acting valve was opened – Fig. 4b. The traverse speed was approximately 1.7m/s and the physical separation of film 1 and the pitot probe was 27mm.

The measurement technique (Section 2.2) requires different surface temperatures on the thin film probes. To generate the different surface temperatures, an external preheating unit was positioned over one of the films, as illustrated in Fig. 1. This preheating unit was swung away just prior to the probes traversing the jet.

The pitot probe, Fig. 1, was a commercial piezoresistive device with a perforated protective screen and an outer diameter of 2.5mm. Manufacturer's data indicates that it should have a uniform response up to 20kHz.

Estimates of the Mach 4 nozzle exit flow parameters are presented in Table 1. These values are based on measurements of the injection static pressure, the pitot pressure, and the flow stagnation temperature measured at x=1mm. Quoted uncertainties are derived from the estimated uncertainties and spatial variation in the static pressure measurements (±3%), pitot pressure (±2%) and stagnation temperature measurements (±2.4%). Note that the uncertainty in static pressure in Table 1 is somewhat lower than the value used in subsequent analyses for stations x=100, 200, and 300mm because of the difficulties in ensuring that the jet static pressure matched the test section environment.

4 Time-averaged Results

4.1 Transient Heat Flux Analysis

The transient thin film heat flux probes provide a measurement of probe surface temperature that must be converted into a heat flux using an appropriate model for the transient heat conduction processes within the probe substrate. For the time-averaged results in the present work, it is important to properly account for the temperature-dependent thermal properties of the quartz because of the elevated surface temperatures encountered during the experiments and the large surface temperature variations that occur as the probe traverses the jet, Fig. 4c. Modelling the hemispherical geometry is also important for the time-averaged results because the heat penetrates a significant distance relative to the probe radius during the 50ms or so taken by the probe to traverse the jet. To accurately model both of these effects, we have used a finite difference solution to the one-dimensional transient heat conduction equation in spherical coordinates which includes the temperature-dependent thermal properties of the quartz (Buttsworth 2001).

The thin film temperature data used in the analysis of the time-averaged results was sampled at about 8kHz, and typical examples of thin film temperature and corresponding heat flux measurements are illustrated in Fig. 4c and d. The time-averaged components of the probe temperature and heat flux data were identified by low-pass filtering the sampled signals such as those illustrated in Fig. 4c and d. The cut-off frequency of the digital filter was varied with the traverse location: 1.0kHz for x=1mm, 0.5kHz for x=100mm, 0.2kHz for x=200mm, and 0.1kHz for x=300mm.

4.2 Stagnation Temperature and Heat Transfer Coefficient Measurements

At each location downstream of injection (x=1, 100, 200, and 300mm), 4 traverses were performed at different initial probe temperatures. In principal, only two different probe temperatures are required for the identification of the flow total temperature and heat transfer coefficient (Section 2.2). However, as the spatial separation of the thin film probes was on the order of 10mm (which is on the same order as the half-width of the jet) the fluctuations in heat flux at the different probes are poorly correlated during a traverse of the jet, and so it is necessary to adopt an RMS analysis for the identification of fluctuations.   While, the motivation for the use of multiple probe temperatures was principally the RMS fluctuation analysis, the analysis of the time-averaged results is also enhanced by the additional data at different temperatures.

To identify the flow stagnation temperature and probe heat transfer coefficient distribution at each traverse location, the time-averaged probe temperature and heat flux data was assembled and a linear regression was performed at each position across the jet. Figure 5 illustrates the regression at two locations across the jet for the traverses at x=300mm.   The intercept of each regression line and the vertical axis indicates the flow stagnation temperature (at that position within the jet) and the inverse of the slope of each regression line indicates the heat transfer coefficient of the probes (at that position within the jet).

The stagnation temperature and heat transfer coefficient results obtained in this manner are presented in Fig. 6 and Fig. 7. The bars illustrated on these figures

indicate the magnitude of the 95% confidence intervals derived from the statistical analysis of the linear regression data (Chatfield 1972). The measurement uncertainty derived from this analysis was around ±5K for the stagnation temperature, and ±3.5% for the heat transfer coefficient at the centre of the jet. Generally, the relative measurement uncertainty in both stagnation temperature and probe heat transfer coefficient increases with distance from the jet center line because the magnitude of the heat flux approaches zero. For example, in the stagnation temperatures reported in Fig. 6d, the stagnation temperatures vary with y only on the order of 10K but the magnitude of bars is clearly larger at y=20mm than at y=0mm. In the heat transfer coefficient results of Fig. 7d, the relative uncertainty increases from about ±3.5% at y=0mm to about ±8% at y=20mm.

The stagnation temperature results in Fig. 6 appear to indicate a drop in stagnation temperature of around 10K towards the outer regions of the jet. Similar spatial variations have been observed in subsonic jet flows (Fox et al. 1993) and also in Mach 2 jet flows (Fox and Kurosaka 1996). Figure 6 also indicates some asymmetry in the stagnation temperature profiles. However, the uncertainties associated with the time-averaged stagnation temperature measurement technique are about ±5K at the centre of the jet, and increase as the outer regions of the jet are approached. Hence, the apparent spatial variations in stagnation temperature may not be significant.

4.3 Heat Transfer Coefficient from Pitot Pressure

Pitot pressure measurements within the jet were combined with static pressure estimates in order to identify the Mach number distributions. Static pressure was taken as equal to the value indicated by the injection static pressure transducer for the traverse at x=1mm, however, for the remaining traverse stations (x=100, 200, and 300mm), the static pressure within the jet was taken as the average of the values indicated by the test section and injection static pressure transducers. Mach number distributions identified from the pitot pressure measurements in this manner are presented as the dots in Fig. 8. Having determined the Mach number distribution, the function described by Eq. (12) was evaluated.

The uncertainty in static pressure is estimated as ±14% at stations x=100, 200, and 300mm and this dominates the uncertainty in pitot pressure (±2%) when deriving the Mach number from the pitot and static measurements. In the centre of the jet, the uncertainty in Mach number is estimated as around ±7%, but at M_∞=1 the uncertainty increases to ±12%.

The function described in Eq. (13) was then evaluated using Sutherland's law for the viscosity and conductivity of nitrogen, assuming the stagnation temperature and the probe temperature were both 290K. As discussed in Section 2.3.2, Eq. (13) is a weak function of the stagnation and probe temperatures. In the present application it was unnecessary to include the actual (measured) stagnation and probe temperatures in the analysis.

The heat transfer coefficient (Eq. 11) was then evaluated with the probe diameter D taken as 3mm. The heat transfer coefficient results obtained in this manner underestimated the experimental values by approximately 2% at the first station, x=1mm. The magnitude of this error is on the same order as the maximum anticipated effects due to variations in T_w (Section 2.3.2), but the sign of the error is different. Treating the jet core flow heat transfer coefficient measurements from this station as calibration data, the effective probe diameter was reduced to 2.88mm in all subsequent calculations. Using this reduced diameter is justified because the fused quartz probe tips are only approximately hemispherical and the radius of curvature is generally less than 1.5mm at the stagnation point (Buttsworth et al. 1998). Furthermore, there are uncertainties in the stagnation point velocity gradient correlations (see Section 2.3.3) that can be accounted for using this calibration procedure. Heat transfer coefficient predictions from the pitot pressure measurements are compared with measurements from the thin films in Fig. 7.

The uncertainties in the thin film measurements of heat transfer coefficient identified in Section 4.2 are representative of the level of agreement between heat transfer coefficient results based on the thin film measurements and the pitot pressure measurements, Fig. 7. In the outer regions of the jet, at say y>20mm, the difference between the thin film and pitot pressure results exceeds the estimated level of

uncertainty in the thin film measurements. In this region, the jet flow is transonic or subsonic (see Section 4.4). Hence, the uncertainty in the heat transfer coefficient derived from the pitot becomes larger in these regions because of the heightened sensitivity to Mach number, as illustrated in Fig. 2. Neglecting uncertainties in the correlation of Section 2.3, the uncertainties in the heat transfer coefficient derived from the pitot pressure and static pressure measurements are around ±1% on the jet centre line but increase to around ±2% when M_∞=1.

4.4 Mach Number and Velocity from Heat Transfer Coefficient

Although $f(M_\infty, \gamma)$ which appears in Eq. (11) is essentially constant in supersonic flows, the pitot pressure varies with Mach number for a given static pressure. Mach number distributions have been calculated from heat transfer coefficient measurements using Eq. (11) in conjunction with the estimated static pressure within the jet. In Fig. 8, the Mach number results that have been derived from the heat transfer coefficient measurements are compared with distributions identified directly from the pitot pressure and static pressure measurements. Based on the previously established uncertainties in convective heat transfer coefficient and static pressure measurements, the uncertainty in Mach number varies from about ±8% on the jet centre line to about ±12% at M_∞=1. The uncertainties in Mach number distributions derived directly from the pitot and static pressure (Section 4.3) are comparable with these uncertainties.

Velocity measurements follow directly from the Mach number measurements since the flow stagnation temperature has already been identified, Fig. 6. Figure 9 illustrates the velocity results derived from the Mach number distributions in Fig. 8. As was the case with the Mach number profiles, the agreement between the velocity profiles identified by the two different methods is very good. On the centre line of the jet, the derived uncertainty in the velocity measurements is about ±2% for both the thin film technique and the pitot probe technique. However, at M_∞=1, the uncertainty in velocity estimated by both techniques increases to around ±10%.

5 Stagnation Temperature Fluctuations

5.1 Transient Heat Flux Analysis

Fluctuations in the stagnation point heat flux were treated in a slightly different manner to the time-averaged stagnation point heat flux measurements. In addition to sampling voltages corresponding to the probe temperatures, signals from heat transfer analogue units (Oldfield et al. 1982) were also recorded. These heat transfer analogue devices were designed to produce a voltage signal proportional to the heat flux assuming a semi-infinite flat plate heat conduction process and constant thermal properties within the film substrate. Although the time-averaged component of the stagnation point heat flux cannot be identified from the temperature signal with such a heat conduction model, it is a reasonable model for fluctuations at frequencies higher than 1kHz. This is because at such frequencies, the heat penetrates only a small distance relative to the probe radius (about 1.5mm), and the associated temperature fluctuations are not large enough to induce significant variable thermal property effects.

Although the fluctuations themselves do not induce significant variable thermal property effects, the time-averaged temperature variations at the probe surface during a traverse of the jet are sufficient to cause significant variations in thermal properties of the substrate. Hence stagnation point heat flux fluctuations were identified from the analogue voltage signals using an analogue sensitivity which varied with the time-averaged probe temperature.

Analogue heat flux signals and the signal from the pitot pressure probe were sampled at approximately 500kHz. Prior to sampling, the pitot pressure signal was low-pass filtered with a cut-off frequency of 60kHz. The analogue devices utilize an active low-pass filter which results in an upper bandwidth of around 85kHz for the heat flux data. After sampling, the heat flux and pitot signals were digitally low-pass filtered with a cut-off frequency of 20kHz (corresponding to a conservative estimate of the pitot probe's bandwidth that remains unaffected by the diaphragm's mechanical resonance). The time-averaged components of each of the high bandwidth signals was identified using the digital filters discussed in Section 4.1. The time-averaged

components were then subtracted from the high bandwidth signals to yield the fluctuating components.

If the total stagnation point heat flux is resolved into mean and fluctuating components,

$$q = \bar{q} + q'$$ (17)

and the heat transfer coefficient and temperatures in Eq. (1) are also resolved in a similar manner, then the fluctuations in the heat flux will be related to the fluctuations in heat transfer coefficient and stagnation temperature according to,

$$\frac{\overline{q'^2}}{\bar{h}^2} \approx \frac{\overline{h'^2}}{\bar{h}^2}\left(\overline{T_0} - \overline{T_w}\right)^2 + 2\frac{\overline{h'T_0'}}{\bar{h}}\left(\overline{T_0} - \overline{T_w}\right) + \overline{T_0'^2}$$ (18)

To achieve the result expressed in Eq. (18), it was necessary to neglect higher order terms and to recognise that the probe temperature fluctuations T_w' are less than 0.4% of $q'/\bar{h}$ for frequencies greater than 1kHz within the supersonic portion of the jet, and hence can also be neglected.

If the heat flux probes are operated at a temperature sufficiently close to the flow stagnation temperature, then Eq. (18) indicates that the stagnation temperature fluctuations can be directly identified from the fluctuations in heat flux and the time-averaged heat transfer coefficient measurements according to,

$$\overline{T_0'^2} \approx \frac{\overline{q'^2}}{\bar{h}^2}$$ (19)

5.2 Results

RMS stagnation temperature fluctuation measurements are presented in Fig. 10 based on the relationship given in Eq. (19) for the four lowest probe operating temperatures which resulted in values of $\overline{T_0} - \overline{T_w}$ of between about -25 and -60K. It can be seen that the differences in apparent stagnation temperature identified using this range of probe temperatures is quite small – the largest differences occur at x=300mm where there is approximately 1K difference in the apparent T_{0rms} over the four probe operating temperatures.

16

To obtain a further indication of the likely accuracy of results presented in Fig. 10, the magnitude of the heat transfer coefficient fluctuations in Eq. (18) was estimated using the pitot pressure measurements. Provided the instantaneous Mach number associated with the fluctuations remains supersonic, the influence of fluctuations in Mach number will be relatively small. If this is the case, Eq. (11) indicates that the fluctuations in heat transfer coefficient will be related to pitot pressure fluctuations according to,

$$\frac{\overline{h'^2}}{\overline{h}^2} \approx 0.25 \frac{\overline{p_{pit}'^2}}{\overline{p}_{pit}^2} \tag{20}$$

Close to the centre of the jet at x=300mm, the RMS pitot pressure fluctuations are around 6% and the RMS stagnation temperature fluctuations are about 1%. Hence, Eq. (20) is probably a reasonable approximation at this position since it is likely that the Mach number will remain supersonic throughout the fluctuations. Close to the centre line of the jet, and for the lowest probe temperature used at x=300mm, the magnitude of the first term on the right hand side of Eq. (18), is estimated with the aid of Eq. (20) as around 7% of $\overline{q'^2}/\overline{h}^2$. This result suggests that a correction of about -0.1K might be applied to the solid line in Fig. 10d. However, this correction has not been applied because it is insignificant relative to the magnitude of T_{0rms} which is about 2.8K at this position. Furthermore, the second term on the right hand side of Eq. (18) involves a correlation of h' and T_0' which may result in either a positive or negative correction to the Fig. 10 results. Estimating the uncertainty in both q' and $\overline{h}$ as ±4% suggests an uncertainty in of about ±6% in T_{0rms}.

7 Conclusions

Time-averaged stagnation temperature and heat transfer coefficient measurements have been used to identify Mach number and velocity profiles within the Mach 4 nitrogen jet. On the jet centre line, the uncertainty in Mach number derived from the heat transfer coefficient measurements was around ±8%. However, the relatively high Mach number at the centre of the jet leads to an uncertainty in velocity measurement of only around ±2%. The jet profiles of Mach number and velocity were also compared with results derived using the pitot probe data. The results

produced by the two different probe techniques are typically in agreement to within the estimated measurement uncertainties.

Measurement uncertainties in the time-averaged quantities become relatively large in the outer (subsonic) regions of the jet because: (1) the transient heat flux becomes low and this results in increased uncertainties in the stagnation temperature and heat transfer coefficient measurements; and (2) measurable quantities such as the pitot pressure and heat transfer coefficient become sensitive to the Mach number away from the hypersonic limit. Although the thin film probe technique described in this article can be applied in flows at any Mach number, the technique holds particular advantages in supersonic flows.

Stagnation temperature fluctuations have also been identified using the transient heat flux data from the thin film probes operated at temperatures close to the time-averaged flow stagnation temperature. The RMS stagnation temperature fluctuations are around 3K in the core of the jet, and increase to over 10K within the jet shear layer. The measurement uncertainty associated with the stagnation temperature fluctuation measurements is estimated as around ±6% or less than ±0.2K at the centre of the jet.

The current work has demonstrated how additional flow parameters such as the Mach number and velocity can be obtained using the transient thin film stagnation temperature probe technique. However, to fully exploit the high bandwidth capabilities of the thin film probes future applications, it may be possible to use probes with a much smaller separation between heated and unheated films such as that described by Buttsworth and Jones (1998b). This would allow instantaneous measurements of stagnation temperature and heat transfer coefficient fluctuations, and largely avoid the need for analysis of the fluctuations in terms of RMS values.

References

Buttsworth DR (2001) A Finite Difference Routine for the Solution of Transient One Dimensional Heat Conduction Problems with Curvature and Varying Thermal Properties. Technical Report Number TR-2001-01, Faculty of Engineering & Surveying, University of Southern Queensland.

Buttsworth DR; Jones TV (1998a) A Fast-Response Total Temperature Probe for Unsteady Compressible Flows. J. Engineering for Gas Turbines and Power 120: 694-702

Buttsworth DR; Jones TV (1998b) A Fast-Response High Spatial Resolution Total Temperature Probe using a Pulsed Heating Technique. J. Turbomachinery 120: 601-607

Buttsworth DR; Jones TV; Chana KS (1998) Unsteady Total Temperature Measurements Downstream of a High Pressure Turbine. J. Turbomachinery 120**:** 760-767

Chatfield C (1970) Statistics for Technology. Penguin.

Fox MD; Kurosaka M; Hedges L; Hirano K (1993) The Influence of Vortical Structures on the Thermal Fields of Jets. J. Fluid Mech. 255: 447-472 (and corrigendum 261: 376)

Fox MD; Kurosaka M (1996) Supersonic Cooling by Shock-Vortex Interatction. J. Fluid Mech. 308: 363-379

Ng WF; Epstein AH (1983) High-Frequency Temperature and Pressure Probe for Unsteady Compressible Flows. Rev. Sci. Instrum. 54: 1678-1683.

Piccini E; Guo SM; Jones TV (2000) The Development of a New Direct-Heat-Flux Gauge for Heat Transfer Facilities. Meas. Sci. Technol. 11: 342-349

Oldfield MLG; Burd HJ; Doe NG (1982) Design of Wide-Bandwidth Analogue Circuits for Heat Transfer Instrumentation in Transient Wind Tunnels. Proceedings 16th Symp. of International Centre for Heat and Mass Transfer, Hemisphere Publishing, pp. 233-257

Schultz D; Jones TV (1973) Heat Transfer Measurements in Short Duration Hypersonic Facilities, NATO Advisory Group for Aerospace Research and Development, AG-165.

VanZante DE; Suder KL; Strazisar AJ; Okiishi TH (1994) An Improved Aspirating Probe for Total-Temperature and Total-Pressure Measurements in Compressor Flows. ASME Paper 94-GT-222.

Vas IE (1972) Flowfield measurements using a total temperature probe at hypersonic speeds. AIAA J. 10: 317-323

White FM (1991) Viscous fluid flow, 2nd ed. New York: McGraw Hill
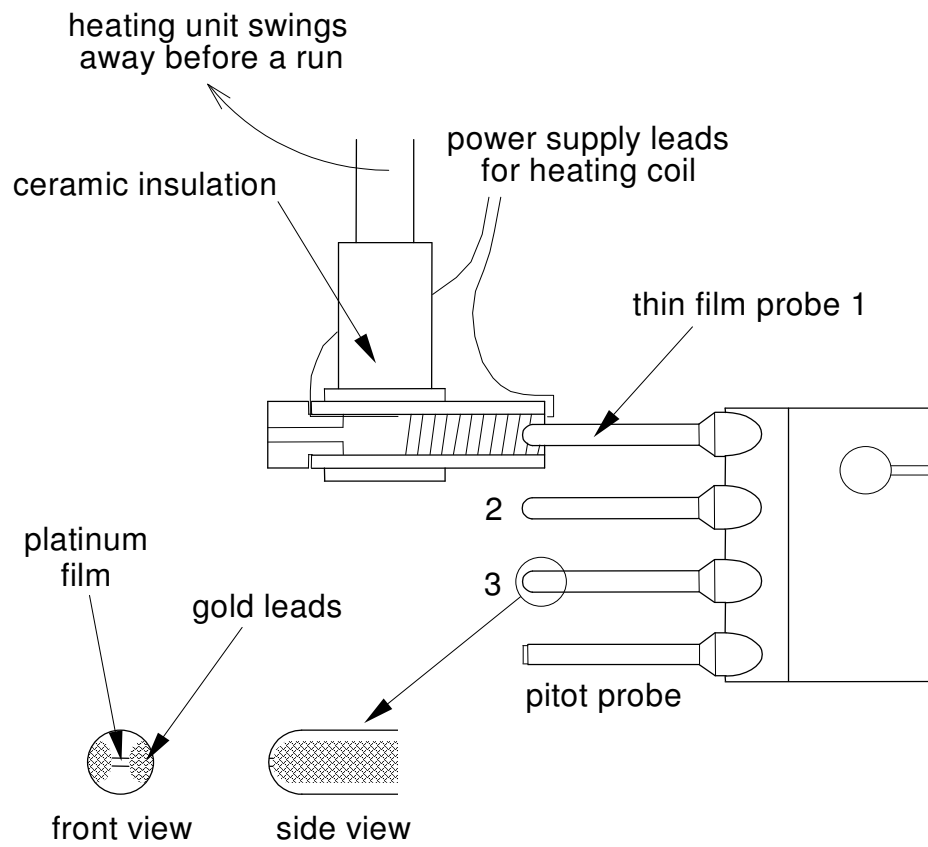
Figure Captions

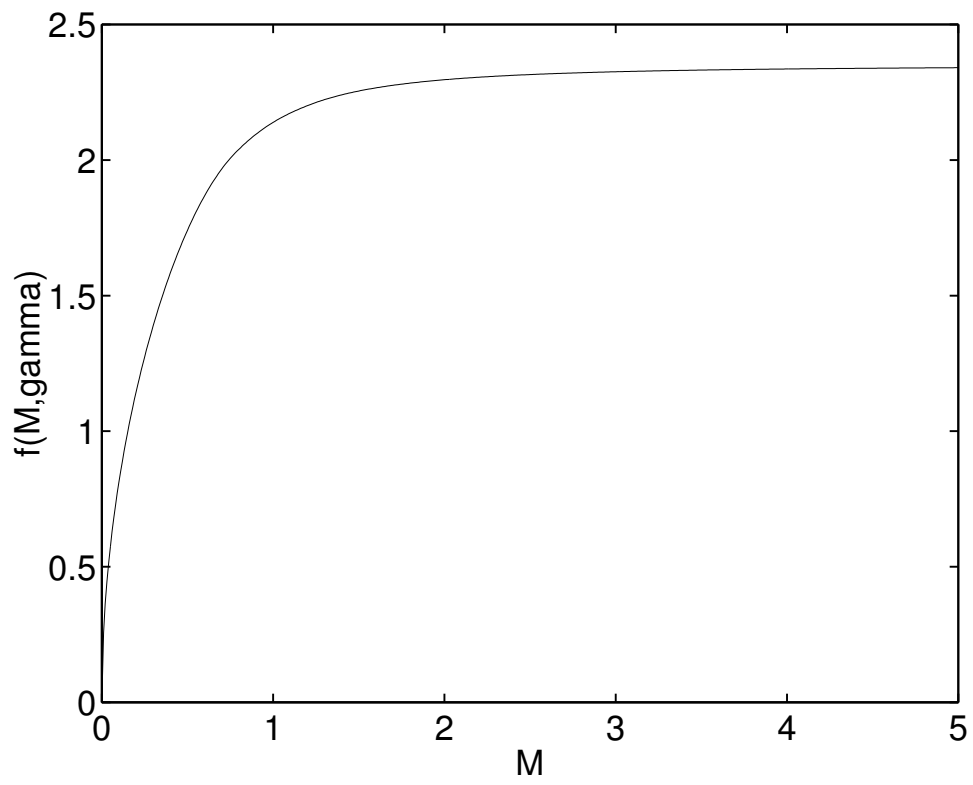**Fig.1.** Illustration of the probe arrangement

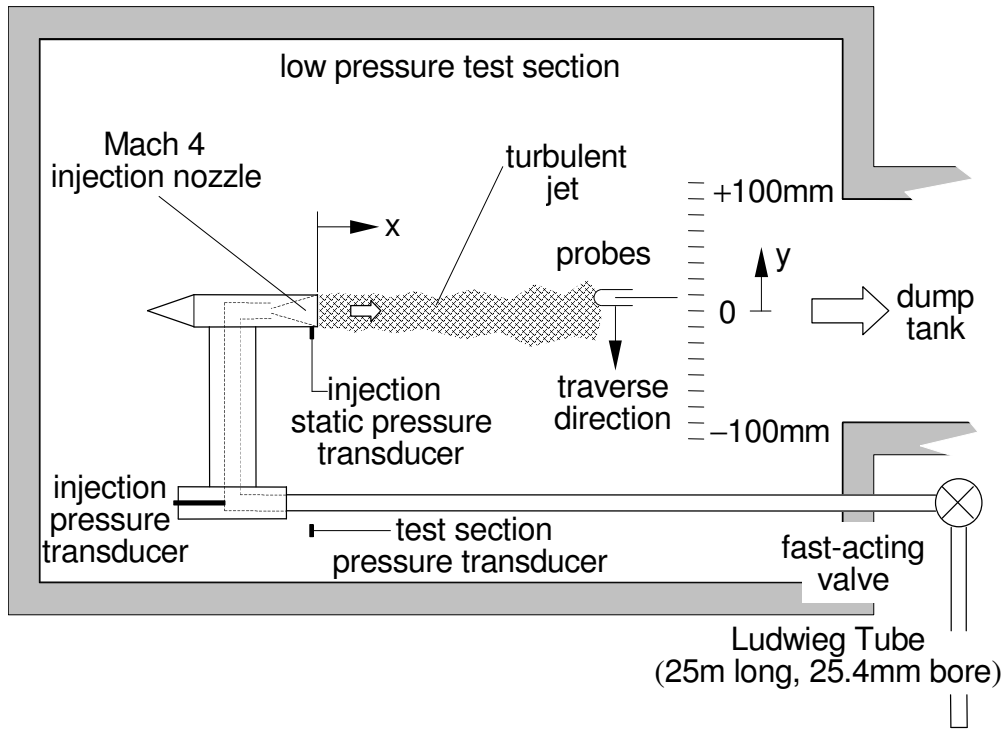**Fig. 2.** Sensitivity of heat transfer coefficient to Mach number as indicated by $f(M_\infty, \gamma)$ for γ=1.4.

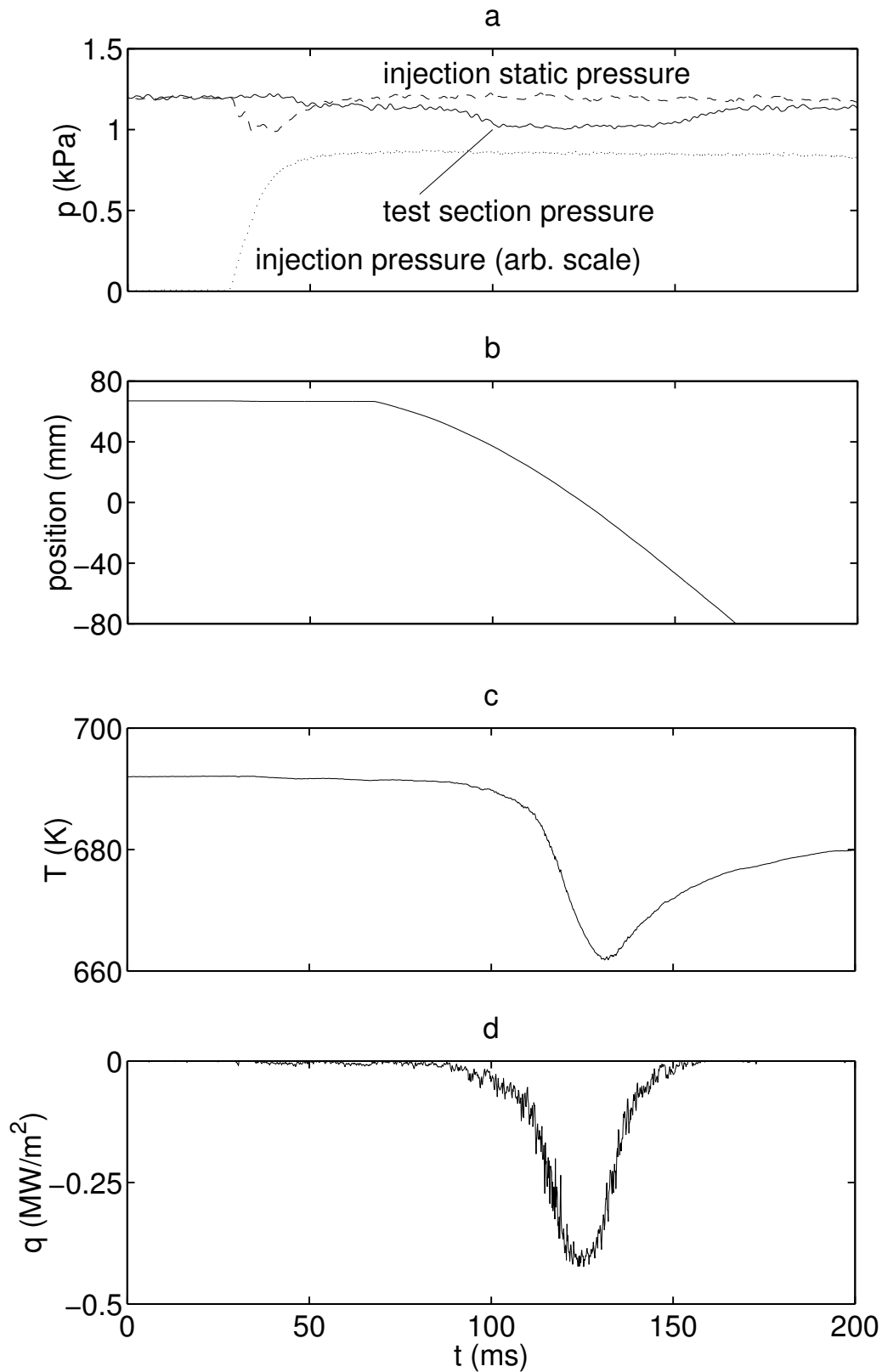**Fig. 3.** Illustration of the Mach 4 free jet arrangement

Fig. 4a-d. Typical signals obtained during an experiment. **a** Pressures; **b** probe displacement; **c** probe tempertures; **d** heat flux
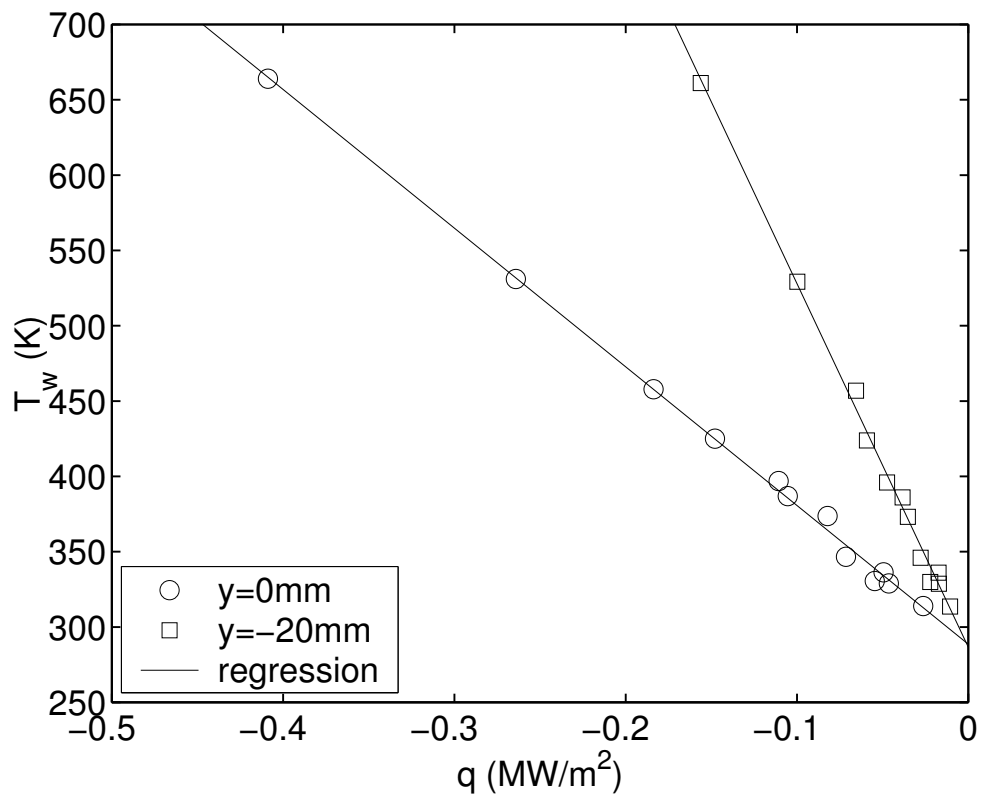
Fig. 5. Illustration of heat flux for various probe tempertures at two locations within the free jet for x=300mm.

Fig. 6a-d. Time-averaged stagnation temperature measurements at 4 stations downstream of injection. **a** x=1 mm; **b** x=100 mm; **c** x=200 mm; **d** x=300 mm

Fig. 7a-d. Time-averaged heat transfer coefficient results at 4 stations downstream of injection. **a** x=1 mm; **b** x=100 mm; **c** x=200 mm; **d** x=300 mm. Solid line: thin film heat transfer coefficient measurements; dots: derived from pitot pressure measurements

Fig. 8a-d. Time-averaged Mach number profiles at 4 stations downstream of injection. **a** x=1 mm; **b** x=100 mm; **c** x=200 mm; **d** x=300 mm. Solid line: derived from heat transfer coefficient measurements; dots: derived from pitot pressure measurements

Fig. 9a-d. Time-averaged velocity profiles at 4 stations downstream of injection. **a** x=1 mm; **b** x=100 mm; **c** x=200 mm; **d** x=300 mm. Solid line: derived from heat transfer coefficient measurements; dots: derived from pitot pressure measurements

Fig. 10a-d. RMS stagnation temperature fluctuations at 4 stations downstream of injection. **a** x=1 mm; **b** x=100 mm; **c** x=200 mm; **d** x=300 mm. Solid line: $\overline{T_0} - \overline{T_w} \approx$ -25K; dots: $\overline{T_0} - \overline{T_w} \approx$ –60K; other lines: intermediate temperatures

Table 1 Mach 4 nozzle injection parameters

Parameter	Value
M_∞	3.7 ± 0.1
T_∞ (K)	78 ± 4
p_∞ (kPa)	1.20 ± 0.04
u_∞ (m/s)	664 ± 10
ρ_∞ ($\times 10^{-3}$ kg/m^3)	52 ± 3

Fig.1. Illustration of the probe arrangement

Fig. 2. Sensitivity of heat transfer coefficient to Mach number as indicated by $f(M_\infty, \gamma)$ for $\gamma = 1.4$.

Fig. 3. Illustration of the Mach 4 free jet arrangement

Fig. 4a-d. Typical signals obtained during an experiment. **a** Pressures; **b** probe displacement; **c** probe tempertures; **d** heat flux

Fig. 5. Illustration of heat flux for various probe tempertures at two locations within the free jet for *x*=300mm.

Fig. 6a-d. Time-averaged stagnation temperature measurements at 4 stations downstream of injection.
a *x*=1 mm; **b** *x*=100 mm; **c** *x*=200 mm; **d** *x*=300 mm

Fig. 7a-d. Time-averaged heat transfer coefficient results at 4 stations downstream of injection. **a** x=1 mm; **b** x=100 mm; **c** x=200 mm; **d** x=300 mm. Solid line: thin film heat transfer coefficient measurements; dots: derived from pitot pressure measurements
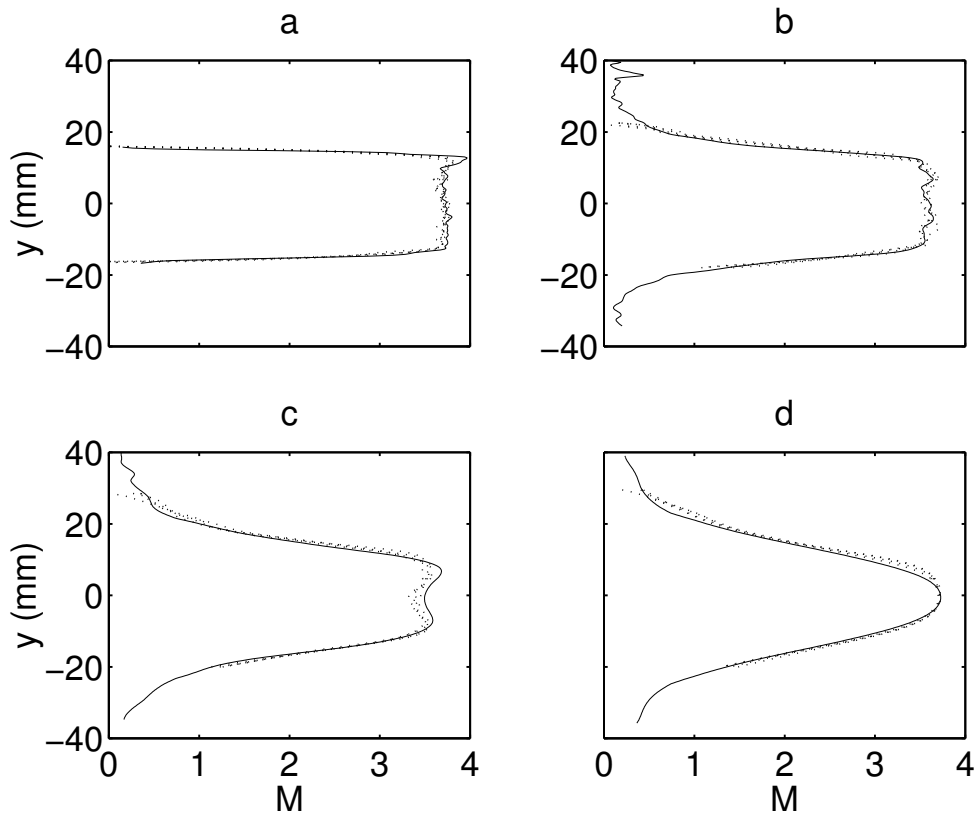
Fig. 8a-d. Time-averaged Mach number profiles at 4 stations downstream of injection. **a** *x*=1 mm; **b** *x*=100 mm; **c** *x*=200 mm; **d** *x*=300 mm. Solid line: derived from heat transfer coefficient measurements; dots: derived from pitot pressure measurements
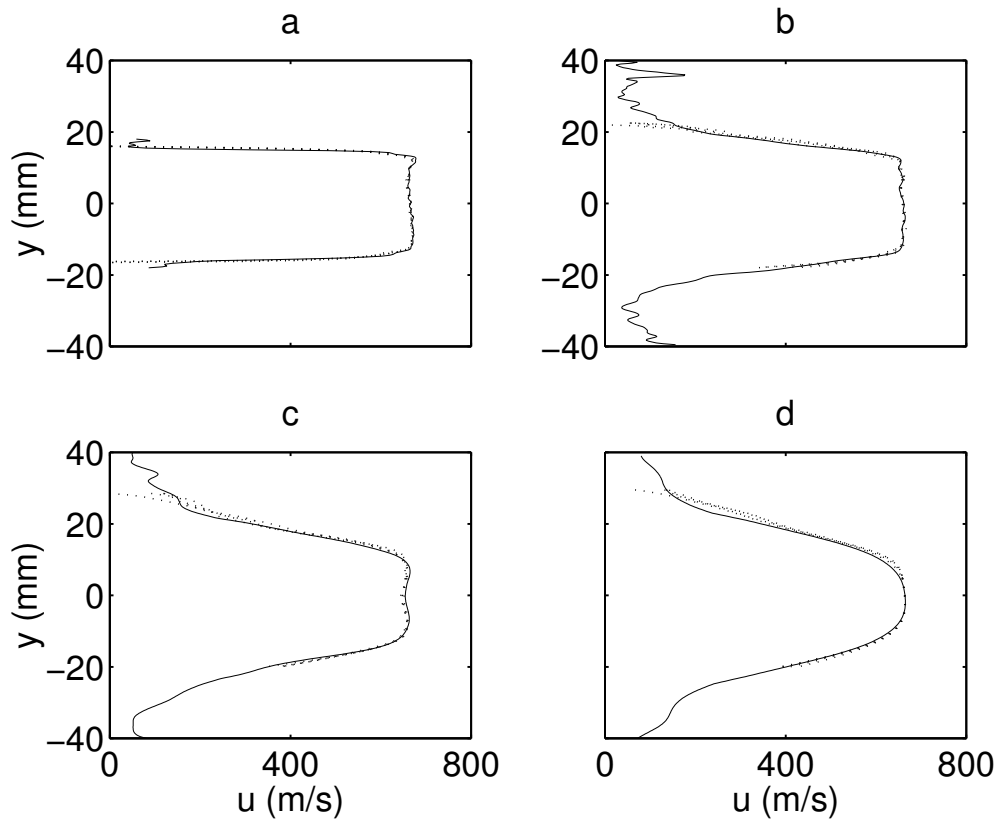
Fig. 9a-d. Time-averaged velocity profiles at 4 stations downstream of injection. **a** x=1 mm; **b** x=100 mm; **c** x=200 mm; **d** x=300 mm. Solid line: derived from heat transfer coefficient measurements; dots: derived from pitot pressure measurements
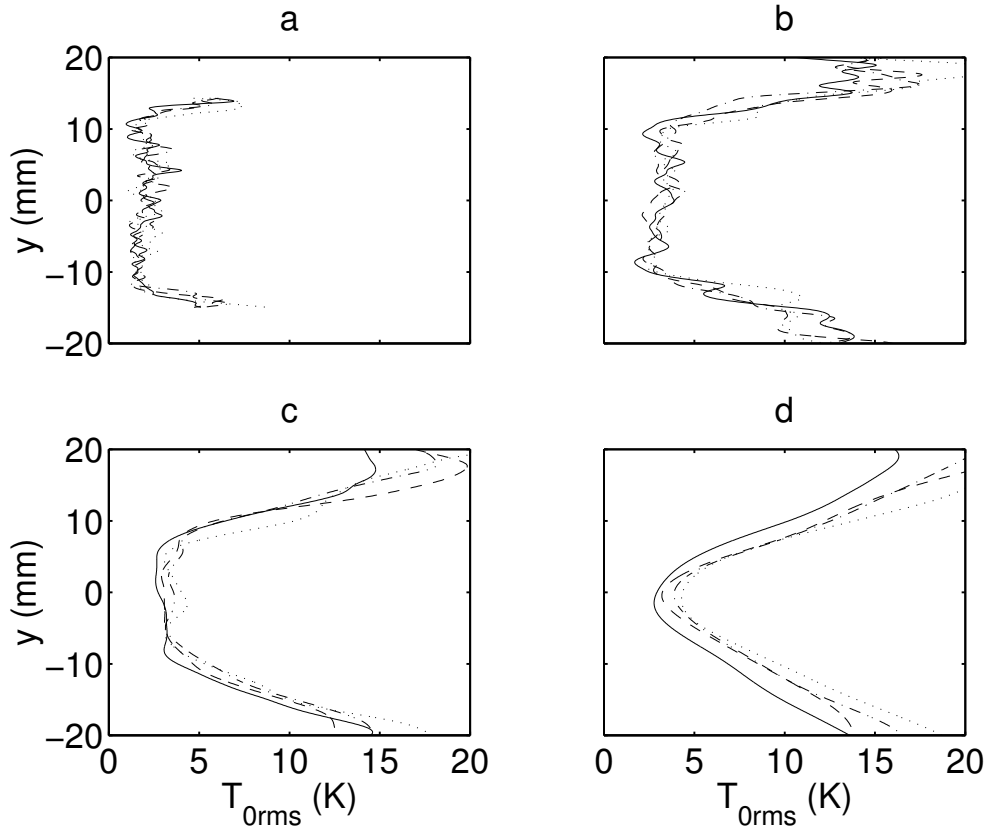
Fig. 10a-d. RMS stagnation temperature fluctuations at 4 stations downstream of injection. **a** x=1 mm; **b** x=100 mm; **c** x=200 mm; **d** x=300 mm. Solid line: $\overline{T_0} - \overline{T_w} \approx$ -25K; dots: $\overline{T_0} - \overline{T_w} \approx$ –60K; other lines: intermediate temperatures